ICWE14
June 21-26, 2015 | Porto Alegre - Brazil
14th INTERNATIONAL CONFERENCE ON WIND ENGINEERING

Mass ratio and afterbody effects in flow-induced vibrations of a 3:2 rectangular cylinder

Massai T.[1], Zhao J.[2], Lo Jacono D.[2,3], Sheridan J.[2]
[1]Department of Civil and Environmental Eng., Faculty of Engineering, Università di Firenze, Firenze, Italy
[2] Mechanical & Aerospace Engineering Department, Faculty of Engineering, Monash University, Melbourne, Australia
[3]Départment de Mécanique, Institut de Mécanique des Fluides Toulouse (IMFT), Université Paul Sabatier, Toulouse, France
email: tmassai@dicea.unifi.it, jisheng.zhao@monash.edu, david.lojacono@imft.fr, john.sheridan@monash.edu

ABSTRACT: The present study aims at describing the evolution of the dynamical response observed for a rectangular section of side ratio (*SR*) 1.5 tested in a low mass ratio (m^*) range. The transition between very low to higher m^* regimes for these reference sections has not been documented yet in the reference literature. A wide experimental campaign was performed in a recirculating water channel to investigate a low m^* regime, using a purposely designed test rig allowing both static and dynamic tests on light cross-sectional models. In particular displacement and force measurements were taken. The *SR* was varied in order to evaluate the afterbody effect on models' aerodynamics and amplitude response. Given that there is evidence for the resultant cross-sections to exhibit a behavior in which VIV and galloping interact in airflow (higher m^*), the possible m^* threshold for which such an interaction takes place was determined. This task was well described and related to *SR* = 1.5, whereas the comparisons with the other sections developed differently though peculiar response branches. The role of interacting higher harmonics of both VIV and galloping is also briefly discussed.

KEY WORDS: VIV; galloping; interaction VIV-galloping; bluff rectangular sections.

1. INTRODUCTION

This study examines the influence of the mass ratio on the response of sharp-edged rectangular cylinders, with three different side ratio (*SR=B/D=0.67*, *1* and *1.5*). *SR* is defined as the ratio between the body width and height facing the oncoming flow (see Figure 1). Considered here is what happens when the bodies are elastically-mounted to allow oscillations transverse to a free-stream flow. Generally speaking a sharp-edged bluff body can be subjected to different forms of aeroelastic phenomena, such as flutter, galloping, and vortex-induced vibrations (VIV). For the *SR* investigated here it has been found that the particular conditions of the geometry that determines the afterbody shapes (defined as the portion of the body after the separation points) and aerodynamic characteristics give rise to two phenomena: VIV and galloping. These two phenomena will be discussed and their mutual interaction investigated.

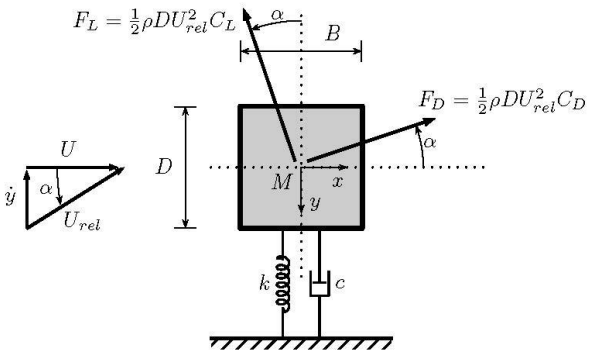

Figure 1. Evaluation of the transverse force on a vibrating rectangular cylinder with the quasi-steady approach. U_{rel} denotes the apparent flow velocity due to the body displacement velocity.

The cross-sections investigated have already been shown to be particularly prone to the interaction between VIV and galloping. ([1], [2]), a dynamic instability of slender non-axisymmetric structures caused by a self-excitation due to the flow. When a cross-section is aerodynamically unstable, according to the Glauert/den Hartog stability criterion, small-amplitude vibrations generate forces that increase the amplitudes to large values as the flow velocity is increased. So far the only suitable theory for predicting oscillations' onset velocity and the post-critical regime is quasi-steady theory, which has been successfully applied in [3]. Once the galloping onset velocity (as shown in Eq. 1.1 reported accordingly respect to the non-dimensionalization chosen in presenting results), which is proportional to the mass and damping ratios, is exceeded the system manifests itself as limit-cycle harmonic oscillations.

$$\frac{U_g^*}{2\pi} = \frac{2\zeta}{nA_1} = \frac{4m\zeta}{\rho D^2 L A_1} = \frac{4\zeta m^* B}{A_1 D}$$

where $m=M/L$ is the mass per unit length and the mass parameter n is expressed in the usual form as equal to $\rho D^2 L/2M$.

In Eq. 1.1 the quasi-steady galloping critical velocity is given as a function of damping (ζ), geometry of the section (B,D), fluid density (ρ), mass ratio (m^*) and slope of the lateral force coefficient around the zero angle of attack, that is $A_1=dC_{Fy}/d\alpha|_{0^\circ}$ (Figure 1 and Eq. 1.2). It is worth noting that even if the quasi-steady theory refers to the n-form of mass ratio expression, an alternative form will be used, $m^*=m/m_d=D/(B2n)$, in which the oscillating system mass (m) is non-dimensionalized with respect to the volumetric mass of the fluid displaced (m_d). If galloping may be referred as a divergent (not self-limited) low frequency aerodynamic instability, generally occurring in a higher range of reduced velocities, one can approximately identify VIV as a self-limited high frequency phenomenon occurring in a bounded lower velocity range. It manifests itself when an elastic or elastically-mounted bluff body is immersed in a moving fluid and the occurrence of a fluctuating pressure distribution on the body may induce a vibrational response at certain velocities.

$$C_{Fy}(\alpha) = -sec(\alpha)\cdot\left[C_L(\alpha) + C_D(\alpha)\cdot tg(\alpha)\right] \tag{1.2}$$

A resonance condition can occur when the vortex shedding frequency, f_{vs}, and that of the body oscillation, f, are locked and close to the system's natural frequency, f_N. The maximum amplitude response, $A^*_{max}=max(A/D)$, where A is the amplitude of the displacement signal, occurs in this lock-in range of $f_{vs} \approx f \approx f_N$, *i.e.* after the reduced velocity increases above, $U_r=1/St$, where St is the fixed cylinder's dimensionless shedding frequency, known as Strouhal number, defined as:

$$St = f_{vs}\frac{D}{U} \tag{1.3}$$

Given that galloping is caused by the aerodynamic forces induced by the transverse movement of the body, there can be no instability without an initial displacement condition. Thus galloping is categorized as a type of *movement-induced vibration*, whereas VIV is categorized as a type of *instability-induced excitation*, given it is associated with the flow instability involving local flow oscillations (see [4]).

Cross-sections of concern in the present work have been assessed previously as being particularly prone to the interaction between VIV and galloping. This interaction was observed from the early 1960s: when a low damped square cylinder was found to start oscillating at the critical velocity of the Kármán-vortex resonance wind speed instead of that predicted by the quasi-steady theory in [1]. Later the interaction was observed and studied in rectangular cylinders with various SR values, *e.g.* in [2] and [5]. It has also been reported that rectangular sections with $SR>1$ are more prone to the interaction [6].

It has been derived that the interaction occurs when the ratio U^*_g/U^*_r is lower than a certain threshold, though the reporting of this shows some variability. In [7] a value of $U^*_g/U^*_r=2.15$ was found to be necessary to separate the phenomena, even if some of the interaction effects were still present for $U^*_g/U^*_r=8.4$. However, in [7] a value of $U^*_g/U^*_r=2.1$ was given.

VIV-galloping interaction is found to be automatically present for $U^*_g<U^*_r$, a condition that is verified for light, slender low-damped structures in air-flow and automatically found in water-flow given the difference in flow density [9]. In such conditions an effect referred to as *quenching* is exerted by the vortex structure on the body until it reaches U_r: this concept comes from non-linear dynamics (*asynchronous quenching*) which was underlined in *e.g.* [10] and [11].

The interaction can manifest itself differently according to experimental conditions and dynamical system properties, *e.g.* in some cases the galloping excitation was seen to start at velocities corresponding to the Kármán-vortex resonance wind speed, instead of 5-6 times larger, or at a wind speed larger than U^*_r but less than one-third of that predicted by the theory ([7], [10]). In [10] tests were conducted aimed at finding the reason for such a behavior. The failure of quasi-steady theory up to very high values of the reduced wind speed and large amplitudes of oscillation was suggested to be due to the effect of interacting Kármán vortices. Here, a range of mass ratios was investigated, via water-flow measurements with different damping/mass ratios related to the square section (SR=1), and for only one value of mass ratio for a SR=2 rectangular cylinder in [11]. It was found the instability onset of the square cylinders developed into galloping oscillations, and this occurred before U_r. This appeared to be a direct result of the interaction with vortex shedding and its onset depended on the mass ratio. A secondary resonance (super-harmonic) was found near $U^*_r/3$, and was more evident for the rectangular section case.

More recently the interaction was approached when a square section was tested in water at several angles of attack ([12]). A transition between galloping and VIV was found by varying the flow incidence and a previously unreported branch of instability was discovered with very high amplitudes of oscillation. In [13] it was shown, as in the case of the square cylinder, a series of 'odd' synchronizations exist for *St* values near odd integer multiple of *f*, during which *f* itself is modified so that a multiple of f_{vs} is synchronized to the body oscillation. An updated review and some new experimental tests on the interference between VIV and galloping in air were given in [14]. This study was focused on *SR*=1.5 and its peculiar features and strong susceptibility to the interaction was underlined, with significant implications in actual codes prescriptions from the practical engineering point of view.

2. EXPERIMENTAL DETAILS

The experiments were conducted in the free-surface recirculating water channel of FLAIR in the Department of Mechanical and Aerospace Engineering at Monash University. The water channel facility has a test section of 4000 mm in length, 600 mm in width and 800 mm in depth. Two bluff body models were used in the present study. A square cross-section rigid cylinder model made from aluminium tubing with a side width of D = 25 mm (*SR*=1) and wall thickness of t =1.6 mm, and a rectangular cylinder of depth D = 24.75 mm, a side width B = 37.45 mm (*SR*=1.5) and a wall thickness of t =2.14 mm. The cylinder can be rotated to $\langle = 90°$ to obtain a *SR*=0.67 cross-sectional model, as shown in Figure 2. The immersed length and aspect ratio calculated based on side length, were L = 778 mm and *AR*=*L*/*D*=31, respectively, for the square section and L = 617.5 mm, and *AR*=25, respectively, for the rectangular cylinder. A 2 mm gap was given between the cylinder's free end and an end- conditioning platform to minimize end effects and to promote parallel vortex shedding.

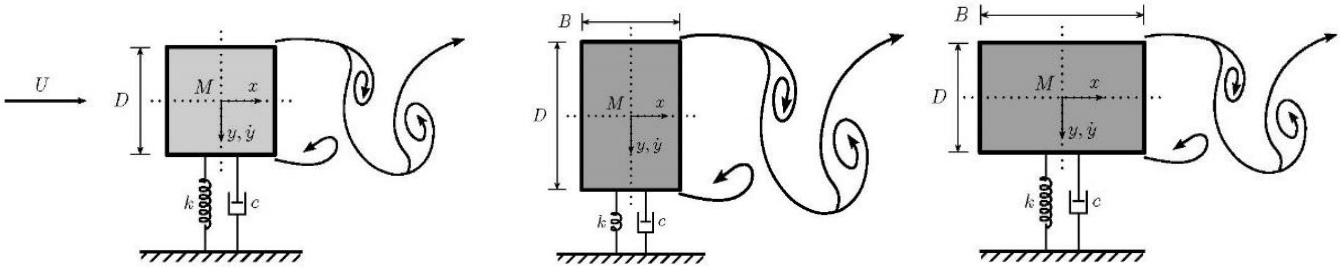

Figure 2. A definition sketch for FIV of a *SR*=1 (left), *SR*=1.5 (center) and *SR*=0.67 cylinders with angle of attack α=0°. The cylinders are allowed to oscillate freely only in the transverse direction *y*, to the oncoming flow *U* in the stream-wise direction *x*.

The cylinder model was vertically supported by a force balance sting that was coupled with a pair of carbon fibre shafts mounted on air bearing bushings. The oscillations were elastically constrained by a pair of extension springs, allowing the cylinder to move with one degree of freedom in the transverse direction to the oncoming flow. A linear variable differential transformer (LVDT) was used to accurately measure the displacement of the cylinder. The lift and drag forces acting on the cylinder were measured using a two-component force balance. For the lift force calculation, the inertial force associated with the body motion was taken into account to yield the instantaneous fluid force, $F_y(t)$. To obtain a reference, the zero position of the cylinder was measured for each test in a quiescent fluid. The references of the forces were obtained in the same way.

The mass ratio for each model was changed incrementally by simply fixing additional masses on the top-moving part of the *air-bearings* rig (Figure 3). The natural dominant frequency of the system was kept close to the reference value of approximately 0.70 Hz by changing the number of spring pairs that elastically connected the stationary parts to the moving shaft of the system. The complete set of test cases tested is shown below in Table 1.

Table 1. Test cases properties for the different *SR* tested: md indicates the fluid displaced mass.

m^*	m [g]	$f_{N,air}$ [Hz]	$f_{N,water}$ [Hz]	Δf %	ζ [%]	*n. springs*
			SR = 0.67 (m_d = 0,571 g)			
2.24	1.28	0.704	0.595	15.4	0.247	2
9.76	4.32	0.565	0.530	6.1	0.145	6
			SR = 1 (m_d = 0.373 g)			
2.64	0.99	0.803	0.65	19.3	0.258	2
11.31	3.73	0.570	0.530	7.0	0.157	4
			SR = 1.5 (m_d = 0.571 g)			
2.24	1.28	0.704	0.519	26.3	0.247	2
9.76	5.58	0.565	0.519	8.1	0.152	6

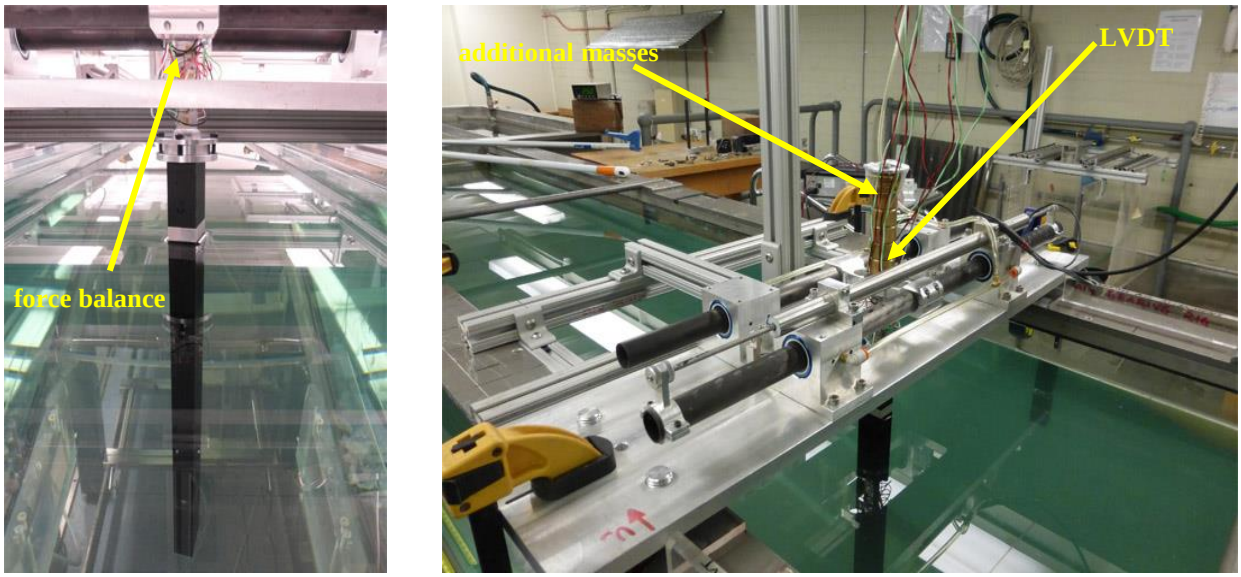

Figure 3. Pictures of the experimental set-up for a cylinder model (*SR*=1.5 mounted).

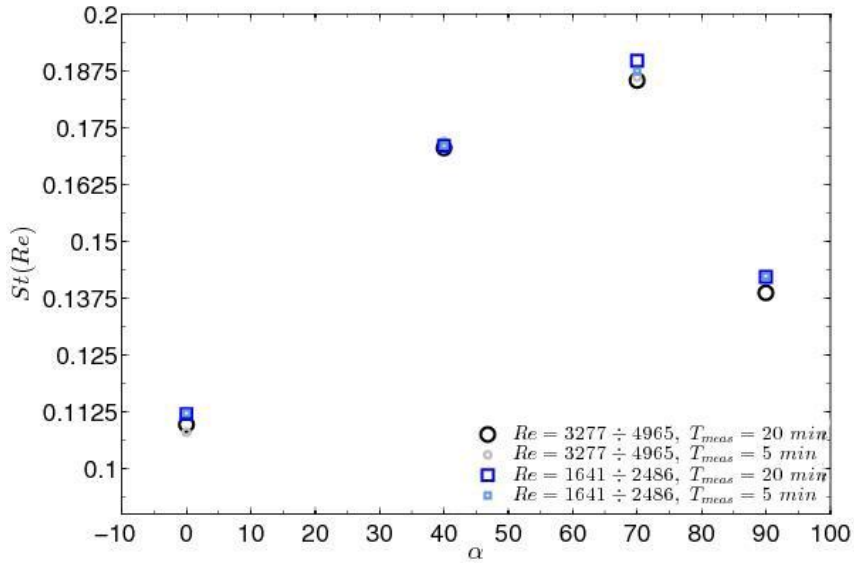

Figure 4. Strouhal number measurements using hot-wire anemometry on the *SR*=1.5 model (α=0°) rotated of three angle of attack positions until reaching *SR*=0.67 (α=90°).

3 RESULTS

The results are given in terms of static and hydroelastic tests conducted in the water channel. Static measurements were necessary to assess the aerodynamic features of the cross-sections for the present work. Hydroelastic responses were measured after having detected the dynamical characteristics of the system through still air and water decay tests (those results are listed in Table 1).

3.1 Static tests

To perform static measurements on each stationary cylinder the shafts supporting the model in the air bearing system were clamped to the channel walls. The force balance connecting the model to the rigid arm was fixed to the moving part of the system in a way that was rigid enough for the purposes of these tests. Static tests were divided into force measurements and *hot-wire anemometry*. The forces measured were used to calculate A_1, as a means for establishing the sensitivity of each section to galloping instabilities. All the three *SR* cases were found to be prone to the instability as soft-type oscillators in water flow, although *SR*=0.67 had been found in air flow to be a hard-type (for more information on the A_1 values of the different sections and further details on static measurements see [15]). In addition, through spectral analysis of the lift coefficient, a first detection of *St* for each angle of attack and for several *Re* values were also obtained. Only the results of the second kind of static test mentioned above is addressed here. A hot-wire anemometer was placed in the near wake of the cylinders, for different angles of attack. Figure 4 shows measurements at four angles of attack (⟨=0°, 40°, 70°, 90°), two flow velocity (meaning two *Re* range), and for two different lengths of recording

(5 and 20 min). It is apparent that the *St* values detected are in good agreement between each other, indicating the reliability of the experimental method. Therefore, the *St* values detected were double-checked with those derived from force measurements, and gave satisfactory results. In summary, the *St* values chose for the three *SR* cases were 0.112, 0.131 and 0.104 respectively for *SR* = 0.67, 1, 1.5. A comprehensive dataset to be compared to these values is reported in [14].

3.2 Hydroelastic tests

Responses of the amplitude and frequency content versus the reduced velocity were examined for the square and rectangular cylinders, where the reduced velocity is defined as $U^*=U/(f_N D)$, where U is the free-stream velocity, and $f_N = f_{nw}$ is the natural frequency of the freely oscillating body within the quiescent fluid. The maximum U^* value for each test case depended on the characteristic length of the body and the natural frequency of the system, being determined by the maximum pump frequency feasible for the water channel. The maximum value for each *SR* was taken as a maximum reference value for graphical results.

3.2.1 Amplitude response

The amplitude response, A^*_{10} is used here (*e.g.* see [12]): it is defined as the mean of the top 10% of the amplitude peaks. This scalar provides a more appropriate and statistically robust measure for comparison of different, independent studies and across different geometries. Compared to A^*_{max}, which gives an extreme measure but is the value of a single sample, A^*_{10} can provide a more meaningful value for assessing the typical amplitudes to consider in determining cyclic loading fatigue. In Figure 5 (*a*), *SR* = 0.67, the response branch can be categorized into three regimes: the first regime is a flow-induced vibrations response with the oscillation amplitude increasing linearly following the Strouhal function line up to $U^* \approx 6$. As the reduced velocity is further increased, a lock-in range occurs for $6 < U^* < 9$, which represents the second regime of the response branch, featured by a low-height lock-in bell that "meets" the beginning of galloping branch with a slight jump downward, which appears to increase linearly with the same slope as the first regime. It is interesting to observe that the higher the mass ratio the greater the jump downwards. Apart from the slight horizontal translation towards higher velocities there are no obvious differences between the three mass ratios tested. Interestingly, the two amplitude response shapes are in good agreement with those shown by Bokaian and Geoola for a *SR* = 0.5 having $9 < m^* < 16$ (see Figure 8 in [16]). As already mentioned, the different behavior of *SR*=0.67 in water and air flow is evidenced in [15].

Square section results have already been carefully addressed in [13] at $m^*=2.64$. They are proposed for two mass ratios in Figure 6 (*a*). They are also in good agreement with those reported in [11] for the square section in water. The onset of the instability is in between the quasi-steady galloping velocity (which is very low in water flow), and the critical velocity. This is caused by the effects of the interaction of the vortex structures and the body motion. Three kinks are observed for $m^*=2.64$: the first kink occurs around $U^*=6$, then a second one at $U^*=16$, while the last one is present around $U^*=22$. It is worth noting that [17] reported the presence of a kink at $U^*=18.84$. A similar shift towards higher reduced velocities with increasing mass ratio is seen for *SR*=0.67.

Figure 7 (*a*) shows results for *SR*=1.5. Again, the amplitude response can be categorized into three regimes, although the amplitude response shape in this case is very different to that of the *SR*=0.67 case. At the beginning, we can observe the presence of a super-harmonic resonance ($U^*<6.5$), with a clearly identified amplitude peak correspondening to $U^* \approx 0.67 U_r$ for $m^*=2.24$. This progressively moves, as the mass ratio is increased, until reaching $U^* \approx 0.6 U_r$ for $m^*=9.76$. Then, a flow-induced vibrations central branch appears, in a de-synchronization regime with decreasing oscillation amplitudes. Lastly, the galloping instability branch starts with a sharp upward jump in the oscillation amplitude. The evolution of the amplitude response branch consists of the shrinking in the de-synchronization central region: in particular, the galloping branch onset velocity get closer and closer to U^*_r as the mass ratio increases. The galloping branch seems to grow at a constant slope, except for the lowest m^* value case showing a linear increase up to $U^*=21$. The jump in amplitude at the instability onset disappears for $m^*>2.24$.

3.2.2 Frequency response

Amplitude response curves should considered with time-frequency spectral energy content to better identify the characteristics and different natures of the response. These are presented beneath the corresponding amplitude response curves, representing the logarithmic-scale frequency power spectrum contour plots of the body oscillation, obtained by taking a Fourier-transform of the time series at a given value of U^*, normalizing the resulting spectrum by the maximum energy, and finally stacking each spectrum next to that obtained at the previous velocity point. This normalization process makes the dominant frequencies at any values of U^* clearly visible, as evident in the sharp and darker continuous lines present in each f^*_{osc} plot. The same procedure has previously been used in other papers, as reported by [13]. It should be noted that the non-dimensional frequency response is defined as $f^*= f^*_{osc} = f/f_N$, which is the ratio between the oscillation frequency and the system's natural frequency.

The response of *SR*=0.67 expresses, for both mass ratios, practically the same behavior. This is more evident in Figure 5 (*b*-*c*), more than in (*a*), the division into three different zones addressed in the last paragraph. An interference of the vortex structure with the galloping instability is seen, which is different to what is observed for higher mass ratio regimes (*e.g.* in air flow), in the first synchronization range following the *St* slope.

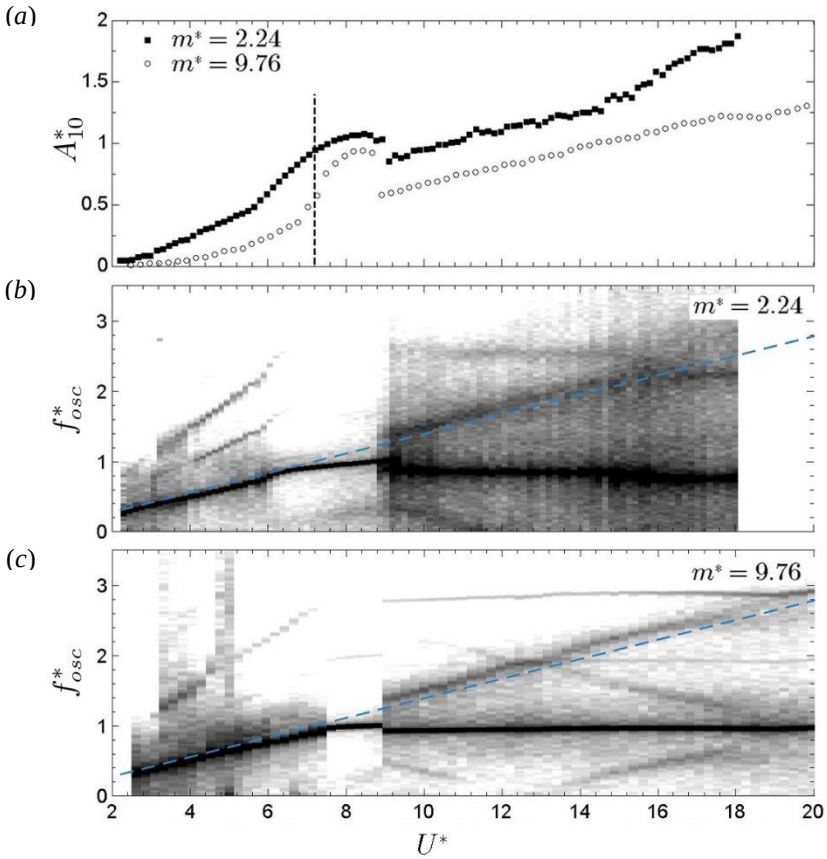

Figure 5. Amplitude response of rectangular cylinders with *SR*=0.67 (*a*): the resonance region is individuated by the sudden amplifications along the instability branch for each m^* value in the vicinity of the dashed lines representing $U^*_r = 1/St$ in A^*_{10} response plot and the reference *St* line in contour f^* maps. The resonance region in (*a*) is correspondingly shown clearly by a distinctive single-frequency response region in (*b*) and (*c*) respectively.

Following this a lock-in region is clearly detected with a less noisy frequency content; finally, the a pure galloping response region develops after the resonance range, characterized by a constant dominant reduced frequency value around 1, and growing oscillation amplitudes as the flow velocity is increased. Given the galloping onset velocity can be theoretically predicted to correspond to an almost zero flow velocity (U^*_g=0.169 and 0.249 respectively for m^*=2.24 and 9.76), one could expect a galloping-type frequency response developing from the beginning of the graph. Here the contour plot is crucial in identifying the first interference region, as it might otherwise have been interpreted as a simple galloping branch had it only been considered from the amplitude response.

Moreover, it it can be observed that the higher (or even lower) harmonics contain, interacting in some cases with each other with consequences for the amplitude response (see below the *SR*=1.5 case for clearer evidence). This aspect differs from one mass ratio to another. In fact, a super-harmonic of order 2 is present in the pure galloping zone for m^*=9.76. This is in addition to one of order 3, as seen in the lower mass ratio test case too, together with a *St* line horizontally flipped around $U^*\approx$12.5. This gives the form a sort of "*X* " trace. The understanding of such behaviour needs further investigations.

Different features in amplitude and frequency responses were observed for the square section. Although the amplitude response can be associated to a classical galloping trend at a first sight, the first two kinks previously mentioned correspond to some features connected to the interaction with vortex shedding. The first kink occurring at U^*=6 represents a small regime of VIV-dominated response, associated with periodic and regular signals compared to the previous and following spectral content. This is different to what happened for *SR*=0.67, nor are there any amplifications in amplitudes in proximity of U^*_r, nor is there a correspondence to the regime expressing periodic flow with a single dominant frequency increasing very slowly and essentially linearly with U^*. This range (11< U^*<14), is a prelude to the second kink (U^*=14-16), showing a weak contribution of the oscillation frequency super-harmonic of order 3. In [13] it was shown the total and vortex lift force contribute significantly, making the vortex shedding synchronized to $3f^*$ in this regime as also reported by [17]. For U^*>16 the frequency response is of the classical galloping type.

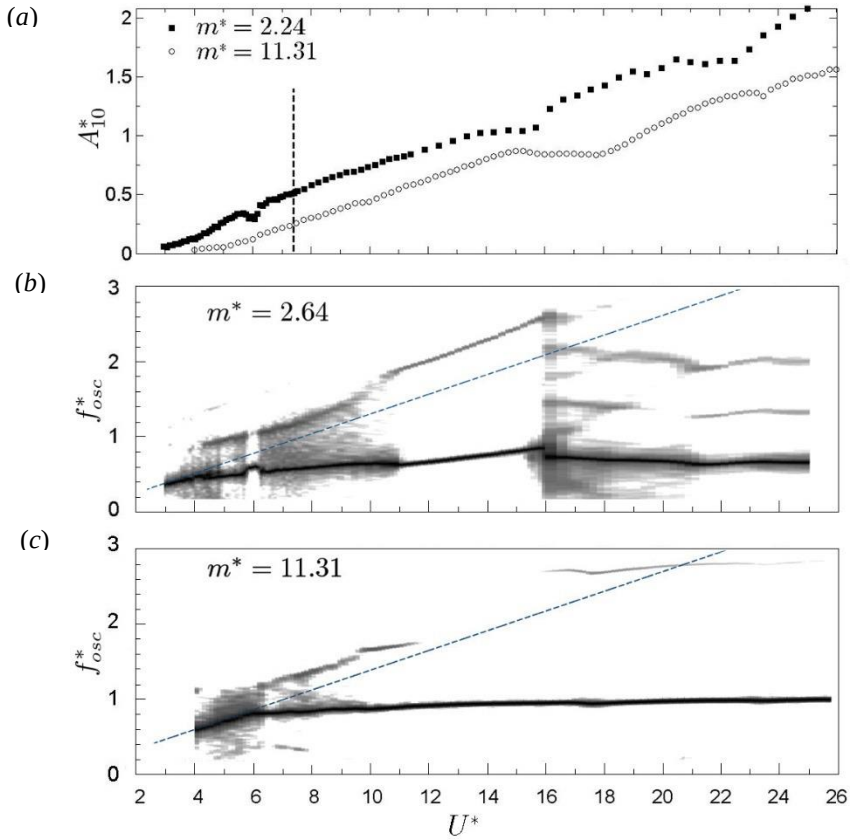

Figure 6. Amplitude response of rectangular cylinders with *SR*=1 (*a*). Resonance regions for m^*=2.64 are individuated by distinctive single-frequency response regions in (*b*).

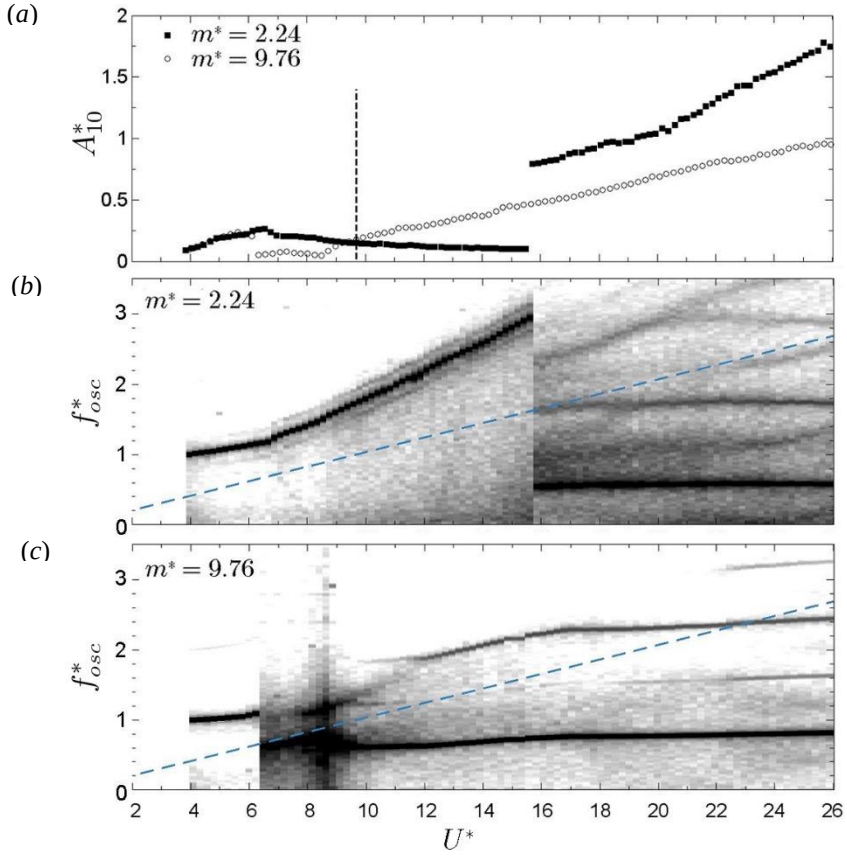

Figure 7. Amplitude response of rectangular cylinders with *SR*=1.5 (*a*): the resonance regions are individuated by the harmonic lock-in single-frequency response regions in (*b*) and (*c*) respectively.

By increasing the mass ratio, the frequency response resembles the classical result. After a synchronization region extending till U^*=6 there seems to occur a lock-in around U^*_r (the slope of the dominant oscillation frequency change from *St* line to almost horizontal, not completely flattened due to the added mass contribution), followed by a pure galloping frequency response range, with amplitudes linearly increasing with U^*. Hence, even if the amplitude response curve seems practically shifted to higher reduced velocities the two situations are very different in frequency content. Figure 7 shows the *SR*=1.5 results. The amplitude response has already been categorized into three regimes, which are also evident in frequency contour plots. The lock-in range occurring at $U^*_r/3$, with an amplitude peak that corresponds to that of U^*_r =0.67 for m^*=2.24, shifts for a higher mass ratio until reaching U^*_r =0.6 for m^*=9.76. A flow-induced vibrations central branch follows this in the de-synchronization regime, with decreasing oscillation amplitudes. Curiously, this central branch has a slope equal to 2*St*. Finally, a galloping instability branch starts with a sharp upward jump in the oscillation amplitude. The interaction with VIV is present here in a peculiar way. For a very low mass ratio, the main instability does not develop from U^*_r, but from higher flow velocity values. Also, the reduced oscillation frequency in the galloping branch is approximately 0.56, which is well below the usual value near the unity. By increasing the mass ratio the de-synchronization range is shrunk, so that the galloping onset gets closer to U^*_r, keeping the same features for even higher values, and increasing also the f^*_{osc} assumed in the galloping regime, which is around 0.8. A similar response was shown in [11] for a *SR*=2 having a mass ratio around 11. Concerning m^*=2.24 it is also worth noting that the interaction between higher harmonics here plays a role in amplifying the response corresponding to the crossing between *St* and the 6th super-harmonic of galloping oscillation frequency response. This does not occur for m^*=9.76.

3. CONCLUDING REMARKS

Extensive experiments have been conducted to study the effect of mass ratio on the flow-induced vibration response of rectangular sections. By starting from a square section the after-body effect has been studied using three different square and rectangular cylinders obtained with two different sectional models and having a comparable minimum mass ratio value. An extremely low mass ratio range has been investigated for the first time, to the authors' knowledge, filling the gap left by previous experiments, in particular for the rectangular cylinders with *SR*=1.5, which have previously been suggested as being particularly prone to the interaction of VIV and the galloping instability. Such interaction has been demonstrated to not occur in the classical way already addressed in literature, depending on the of the cross-sections' *SR* and their mass ratio, which have a role in the amplitude and frequency type response of the investigated bodies. The after-body effect is demonstrated to have a crucial role for the instability onset and the overall response shape, with the three *SR* tested showing completely different peculiarities in their responses.

REFERENCES

1. G. Parkinson and P. Brooks, On the Aeroelastic Instability of Bluff Cylinders, Transaction of ASME, p. 252-258, 1961.
2. J.D. Smith, An experimental study of the aeroelastic instability of rectangular cylinders, Ma.Sc. Thesis, University of British Columbia, 1962.
3. G. Parkinson and J. Smith, The square prism as an aeroelastic non-linear oscillator, The Quarterly Journal of Mechanics and Applied Mathematics, v. 17, p. 225-239.
4. M.P. Païdoussis, Fluid-Structure Interactions. Slender Structures and Axial Flow, ELSEVIER, Volume 1, p. 1-572, 1998.
5. M. Novak and H. Tanaka, Effect of Turbulence on Galloping Instability, Journal of the Engineering Mechanics Division - Proceedings of the ASCE, v. 100, p. 27-47, 1974.
6. M. Novak, Galloping oscillations of prismatic structures. J.Eng.Mech.Div.98 (1), p. 27–46, 1972.
7. G. Parkinson and M. Wawzonek, Some considerations of combined effects of galloping and vortex resonance, Journal of Wind Engineering and Industrial Aerodynamics, v. 8, p. 135-143, 1981.
8. C. Scruton, On the wind-excited oscillations of stacks, towers and masts, In: Wind Effects on Buildings and Structures: Proceedings of the Conference Held at the National Physical Laboratory, Teddington (UK), 1963. HMSO, London, p. 798–837, 1965.
9. G. Parkinson, Phenomena and modelling of flow-induced vibrations of bluff bodies, Progress in Aerospace Sciences, v. 26, p. 169-224, 1989.
10. T. Santosham, Force measurements on Bluff Cylinders and Aeroelastic Galloping of a rectangular Cylinder, University of British Columbia, 1966.
11. D. Bouclin, Hydroelastic oscillations of square cylinders, University of British Columbia, 1977.
12. A. Nemes, J. Zhao, D. Lo Jacono and J. Sheridan, The interaction between flow-induced vibration mechanisms of a square cylinder with varying angles of attack, Journal of Fluid Mechanics, v. 710, p. 102-130, 2012.
13. J. Zhao, J.S. Leontini, D. Lo Jacono and J. Sheridan, Fluid-structure interaction of a square cylinder at different angles of attack, Journal of Fluid Mechanics, v. 747, p. 688-721, 2014
14. C. Mannini, A.M. Marra and G. Bartoli, VIV-galloping instability of rectangular cylinders: Review and new experiments, Journal of Wind Engineering and Industrial Aerodynamics 132, 109-124, 2014.
15. T. Massai, On the Interaction between vortex-induced vibrations and galloping in rectangular cylinders of low side ratio, Ph.D. thesis, Florence/Braunschweig, Italy/Germany, University of Florence/ Technische Universität zu Braunschweig, 2015.
16. A. Bokaian, F. Geoola, Effect of vortex-resonance on nearby galloping instability, Journal of Engineering Mechanics, v. 111, n.5, p. 591-609, 1985
17. P. Bearman, I. Gartshore, D. Maull and G. Parkinson, Experiments on flow-induced vibration of a square-section cylinder, Journal of Fluids and Structures, v. 1, p. 19-34, 1987.